Latin American Journal of Aquatic Research, 53(5): 801-822, 2025
DOI: 10.3856/vol53-issue5-fulltext-3481

Research Article

Field observations of wave and current dynamics on a microtidal dissipative-intermediate environment at Bocagrande Beach Colombian Caribbean during dry and wet seasons

Julie Ruiz-Merchán[1,2,3], Juan C. Restrepo[1], Brian K. Haus[2,3], Luis Otero[1] Mario Conde-Frías[1], Jairo Cueto[4,7], Margarita Guerrero[5], Anlly Melissa Guerrero[1] Cesar Tovio[1] & Marco Vega[4,6]
[1]Geosciences Research Group-GEO4, Department of Physics and Geosciences
Universidad del Norte, Barranquilla, Colombia
[2]Alfred C. Glassell Jr. Sustain Laboratory, Rosenstiel School of Marine, Atmospheric, and Earth Science, University of Miami, Rickenbacker Causeway, Miami, USA
[3]Department of Ocean Sciences, Rosenstiel School of Marine, Atmospheric, and Earth Science
University of Miami, Rickenbacker Causeway, Miami, USA
[4]Department of Natural and Exact Sciences Research Group in Natural and Exact Sciences-GICNEX
Universidad de la Costa, Barranquilla, Colombia
[5]Faculty of Science, Education, Arts, and Humanities, Institución Universitaria de Barranquilla
Barranquilla, Colombia
[6]Department of Civil Engineering, Faculty of Engineering, Universidad Simón Bolívar
Barranquilla, Colombia
[7]Coastal Geology and Sedimentology Group, Institute of Geosciences
Kiel University, Kiel, Germany
Corresponding author: Julie Ruiz-Merchán (merchanj@uninorte.edu.co)

ABSTRACT. The surf zone is one of the most dynamic coastal regions, primarily driven by the interplay of cross-shore velocity (u), alongshore velocity (v), gravity (G), and infragravity (IG) wave oscillations, which significantly impact the movement of water and sediment within the surf zone. This study presents field observations of wave and current dynamics on a microtidal dissipative-intermediate beach on the Colombian Caribbean coast during dry and wet seasons. Through the application of continuous wavelet transforms to pressure sensor data and current meter data recorded in field campaigns, the contributions of G and IG waves to the evolution of free surface elevation (η) and current velocities (u and v) were analyzed; observed along the intermediate-dissipative Bocagrande Beach, Colombia coast, which was impacted by flooding and erosion during two climatic wet and dry periods. Results indicated that, during the dry period, cross-shore and alongshore standing leaky waves were recorded in the parts of the beach both nearest and farthest from the shore. In the area nearest to the shore, cross-shore and alongshore standing edge waves were observed, as the beach lies between two groins. On the other hand, cross-shore and alongshore progressive leaky waves prevailed near shore during the wet period. Spectral analysis indicated that G-wave energy decreases shoreward, while IG energy increases, dominating alongshore currents. These findings underscore the importance of incorporating alongshore variability into studies of coastal dynamics, thereby facilitating a deeper understanding of the roles played by gravity and infragravity waves in sediment transport processes.

Keywords: infragravity waves; gravity waves; edge waves; leaky waves; surf zone, microtidal

Associate Editor: Sergio Neira

INTRODUCTION

The surf zone is one of the most complex and dynamic regions of the coastal environment due to the wide range of wave scales involved. Most swell energy originates from gravity (G) waves, as these waves approach the coast, water depth and wave propagation velocity decrease. When sufficiently shallow depths are reached by G waves, this break generates the currents and turbulent bore characteristic of coastal zones. In the bore, a large portion of the energy is dissipated through turbulence, simultaneously releasing an infragravity (IG) wave, which increases in energy as it is not associated with a group of waves (Beach & Sternberg 1988, Thomson et al. 2006).

Within the surf zone, nonlinear processes transfer energy from high-frequency waves to low-frequency ones (Huntley 1976, Guza & Thornton 1982). These wave categories are distinguished according to their period. High-frequency waves, known as G waves or short waves, have periods between 1 and 30 s, whereas the period of low-frequency waves, known as IG waves or long waves, ranges from 20 to 300 s (Munk 1949, Tucker 1950). The mechanisms generating free IG waves have been studied since the first observations made by Munk (1949) and Tucker (1950). Some studies have shown that such mechanisms can be explained by the release of a forced long wave (Masselink 1995, Ruju et al. 2012), as previously proposed by the theoretical approach of Longuet-Higgins & Stewart (1962). According to the model presented by Symonds et al. (1982), free IG waves are generated by spatiotemporal variations of the breaking point associated with groups of short waves (Pomeroy et al. 2012).

There are two main generating mechanisms of IG waves. In the first, known as bound long waves (Longuet-Higgins & Stewart 1962, 1964), IG waves are produced by nonlinear interactions between G waves outside the surf zone. In other words, the generation of IG waves is related to the presence of groups of short waves, formed by superposing two different wave trains with unequal wavelengths but similar frequencies. The amplitudes of both waves are summed when they are in phase and diminished when they are out of phase, producing a wave group structure that results in a linked long wave. The second mechanism, termed time-varying breakpoints (Symonds et al. 1982), is based on a model for generating low-frequency swell on variable sea bottoms. In this case, the generating mechanism considered by the model is the displacement of the breaking point. Both generation mechanisms are complementary and can coexist, establishing a complex pattern that is difficult to differentiate (Schaffer 1994). However, according to Battjes et al. (2004), the relative importance of either mechanism is related to beach slope. Bound long waves will dominate in low-slope beaches, whereas time-varying breakpoints will prevail in high-slope beaches (Baldock et al. 2000, Baldock & Huntley 2002).

IG waves can be classified into three categories: forced long waves (also known as bound long waves), leaky waves, and edge waves. Before breaking, low-frequency oscillations may move as forced long waves, linked to the generation mechanism on which they depend. After breaks, they can be regarded as free waves, given that the forced long wave is released and can maintain itself. Free waves may be either leaky waves that, after wave breaking, are reflected offshore or edge waves coming from the reflection of free waves on the beach and trapped on the coast by refraction (Longuet-Higgins & Stewart 1962). Both leaky and edge waves may, in turn, be either progressive or standing or be oriented either cross-shore or alongshore (Huntley 1976, Holman 1981, Péquignet et al. 2009).

Another type of IG wave, differing in nature from those mentioned previously, is shear waves, also known as far IG waves. These waves, characterized by having longer periods (~>500 s), are produced by the instability of alongshore currents (v) caused by discontinuities present within them. The expression "leaky waves" refers to a long wave that originates from bound waves being reflected off the coast and propagating offshore, allowing the sea bottom not to trap them. Even though this term refers only to reflected long waves, it is also used for standing leaky waves, which form in the surf zone due to the superposition of two progressive waves (one onshore, another offshore). In other words, standing leaky waves are generated by the simultaneous presence of onshore propagation and reflection of progressive leaky waves. However, what distinguishes standing leaky waves from edge waves (which are a three-dimensional phenomenon) is their standing oscillation pattern, related to offshore IG waves that exhibit little alongshore variation (Guza & Thornton).

Edge waves, as well as leaky waves, come from bound waves that are reflected on the beach and trapped on the coast due to refraction. They are formed by the reflection of incident and IG waves and refraction over an irregular sea bottom. These waves propagate alongshore and are common in areas with sharp changes in the coastline. In the cross-shore direction, these waves can be progressive or standing by means of

the superposition of opposing standing waves. A feature of edge waves that makes them important for fully dissipative beaches is that, when trapped nearshore, they cause an exponential decay in amplitude in an offshore direction (Guza 1974). However, on those beaches where bars are present, edge waves may be trapped and amplified depending on the location of the bar (Bryan & Bowen 1996, Henderson & Bowen 2003). In these cases, the maximum amplitude of the wave is reached on the bar crest, followed by an exponential decay of the wave from the sea to the bar. On the other side, Bowen & Inman (1969, 1971) indicated that periodical variations in features such as *cusps* and rip currents along the coast are formed as a result of interactions between edge waves and the coast.

Previous works have shown that the importance of incidentally forced long waves, generated at the breaking point, depends both on incident swell conditions and the sea bottom profile. In addition, the energy associated with IG waves has a significant effect, particularly nearshore, since it can influence the evolution of free surface elevation (η) dynamics and the pattern of cross-shore velocity (u), alongshore velocity (v) produced by wave breaking. This influence on η and currents, in turn, produces variations in sediment transportation, promoting morphological change (Carter et al. 1973, Aagaard et al. 2013).

Contributions from previous studies enable the assessment and classification of nearshore IG wave types, considering the phase relationships between η, u, and v at any given location where these variables are measured (Huntley 1976, Holman 1981, Péquignet et al. 2009, Winter et al. 2017). In this way, for standing edge waves, both cross-shore and alongshore, there is a 90° mismatch between velocities (u, v) and η, whereas the mismatch between u and v is either 0 or 180° (Huntley & Bowen 1973, Guza & Thornton 1985). Regarding cross-shore and alongshore progressive leaky waves, both velocities (u and v) are in phase with η at 0°, whereas velocities (u and v) are in phase with each other at either 0 or 180° (Huntley & Bowen 1973, Goodfellow & Stephenson 2008).

The work of Winter et al. (2017) features a new view on the impact of an alongshore irregular seabed on IG waves and the propagation patterns produced by these waves. Therefore, a variable nearshore sea bottom, which often occurs along rocky reef shores, may produce standing wave patterns both alongshore and cross-shore. In agreement with this, beaches with a dissipative profile are a favorable scenario for the release of forced IG waves, which in turn transform into leaky waves that influence cross-shore sediment transport (Wright et al. 1991). Nevertheless, a dissipative beach with intermediate traits may generate edge waves.

This work builds upon previous research on various aspects of the same study area. These studies have yielded differing results (e.g. IG oscillations, hydrodynamics, morphodynamics), primarily due to the diverse conditions found on these beaches throughout the year. Among these previous studies, Conde-Frias et al. (2017a,b) focused on the surf and swash zones, using a numerical model to assess the relationship between G and IG energies to replicate how swell transforms as it approaches the coast in the surf zone of a dissipative beach. In this way, the authors revealed that the swell IG energy band is not dissipated in the surf and swash zones, implying that the lack of low-frequency swell reflection allows the water lamina to reach further onshore. Lastly, the results highlight the need for complementary analyses that allow a deeper understanding of the role that IG waves play in beach sediment transport.

The study of Montaño-Muñoz (2015) in Bocagrande Beach analyzed swash zone oscillations and IG wave behavior using field data and camera system analysis. The study found that IG energy dominates the swash spectrum under calm conditions; however, it did not provide a comparative analysis between different weather seasons. Spectral signatures showed that IG energy prevails in oscillation spectra. Furthermore, the study by Montaño-Muñoz et al. (2018) employed an approach that analyzed patterns of velocity and sediment transport. One of the results was that at Bocagrande Beach, velocities v was similar in magnitude and direction to velocities u, which can be attributed to the presence of edge waves between the two groins. Nevertheless, more studies are needed to verify this hypothesis.

Previous research by Ruiz-Merchán et al. (2019), through the application of cross-wavelet transform (XWT) and wavelet transform coherence (WTC), identified IG energy on a microtidal intermediate-reflective beach. The study analyzed the role of G and IG waves in determining beach dynamics over two distinct climatic periods, using a continuous wavelet transform. During the dry period, significant concentrations of IG energy were observed near the coast, driven by reflection processes. The analysis revealed the presence of both cross-shore and alongshore standing "leaky" and "edge" waves. In contrast, during the wet period, progressive leaky waves became more prominent further offshore, while

nearshore areas exhibited leading standing leaky waves. In fact, Costa Verde Beach, characterized by plunging wave breaks typical of intermediate-reflective beaches, undergoes seasonal morphological changes.

During the wet season, the beach exhibits an intermediate ridge-runnel configuration. In contrast, in the dry season, it assumes a cross-shore bar and rip beach profile, characterized by small rip currents and distinct *cusps*. However, correlations with standing edge waves remain uncertain. To obtain these results, Ruiz-Merchán et al. (2019) conducted four-day field campaigns in both the dry and wet seasons, during which pressure sensors and acoustic current meters were deployed in the surf and shoaling zones to record pressure and the velocity components (u, v) across the beach. Pressure records were converted into η using linear transfer functions and corrected for trends and tidal contributions, after which the time series were band-pass filtered and organized into analysis windows for classical spectral analysis (Fourier) and non-stationary analysis using continuous wavelet transform (CWT), enabling the characterization of the temporal and frequency distribution of energy at both G and IG bands.

Furthermore, XWT and WTC techniques were applied to assess phase relationships between η and the velocity components (u, v), allowing the identification of different types of IG waves in the surf zone. Additionally, bathymetric and shoreline surveys were conducted during both the wet and dry seasons, one day before the installation of the measuring equipment. These surveys, complemented by wave propagation simulations using the SWAN model -previously calibrated and validated for the Colombian Caribbean coast- along with Iribarren numbers calculated from WWIII reanalysis wave conditions and the dimensionless sediment fall parameter (Ω), allowed for a comprehensive characterization of the beach's morphodynamic state.

The majority of research on the evolution of low-frequency waves in coastal areas has focused mainly on mesotidal and macrotidal beaches. In contrast, the mechanisms of IG wave generation on microtidal beaches have been comparatively less studied (Melito et al. 2022). This manuscript expands the understanding of IG wave dynamics on an intermediate-dissipative microtidal beach by collecting *in situ* data during two contrasting climatic seasons. Then, based on the results obtained, an analysis is conducted of the patterns of IG wave energy evolution and their relationship to the formation of circulatory systems in the surf zone (Winter et al. 2017, Ruiz-Merchán et al. 2019). Thus, the present study evaluates the contributions of both G and IG waves to variations in current velocities (u and v) along both the alongshore and cross-shore directions at Bocagrande Beach. Correlation analysis and wavelet coherence techniques are also employed to explore the relationships between velocity components (u, v) and η in the surf zone.

The primary objective of this study is to enhance the understanding of wave-current interactions in the surf zone of a dissipative-intermediate, microtidal beach under varying wet and dry climatic conditions. This paper has two objectives. The first is to assess the contributions of G and IG wave regimes in the formation of currents (u, v) within surf zone circulation systems. The second is to identify the IG wave patterns present under these contrasting conditions. Together, these objectives provide new insights into the processes controlling circulation and wave dynamics in highly energetic coastal environments.

MATERIALS AND METHODS

Study area

Bocagrande Beach is located on the Caribbean Coast of Colombia, in the city of Cartagena (Figs. 1a-b). Bocagrande is composed of small, closed beaches bounded by groins. The study area is on the southern end of the coast in Bocagrande, from the first groin (known as Iribarren) to the second one, encompassing approximately 250 m of shoreline (Fig. 1d).

Bocagrande is a microtidal beach with a dissipative-intermediate profile, a wide surf zone, and a high-energy regime. The slope is 0.003 (tanβ) offshore and 0.018 (tanβ) foreshore (Conde-Frias et al. 2017a). The sediment is medium-grained sand, with diameters ranging from 0.08 to 0.42 mm, and a mean diameter of 0.15 mm (Cueto & Otero 2020). The beach is composed of medium-grained, terrigenous, quartz-rich sands derived from continental erosion and fluvial inputs (Posada & Henao 2008, Restrepo & López 2008). A sediment density of $\rho_s = 2650$ kg m^{-3}, consistent with quartz-dominated sands, and the dynamic viscosity of seawater is $\mu \approx 1.0\times10^{-3}$ Pa s at 25°C (Sharqawy et al. 2010). Due to its characteristic dissipative profile (Fig. 1c), Bocagrande Beach is exposed to erosive processes, as evidenced by the shoreline retreat in response to extreme events (Cueto & Otero 2020). Due to this response, and in accordance with the influence of waves, winds, and weather seasons, berms appear and disappear on the beach. The formation and destruction of berms create a potential area for flooding, depending

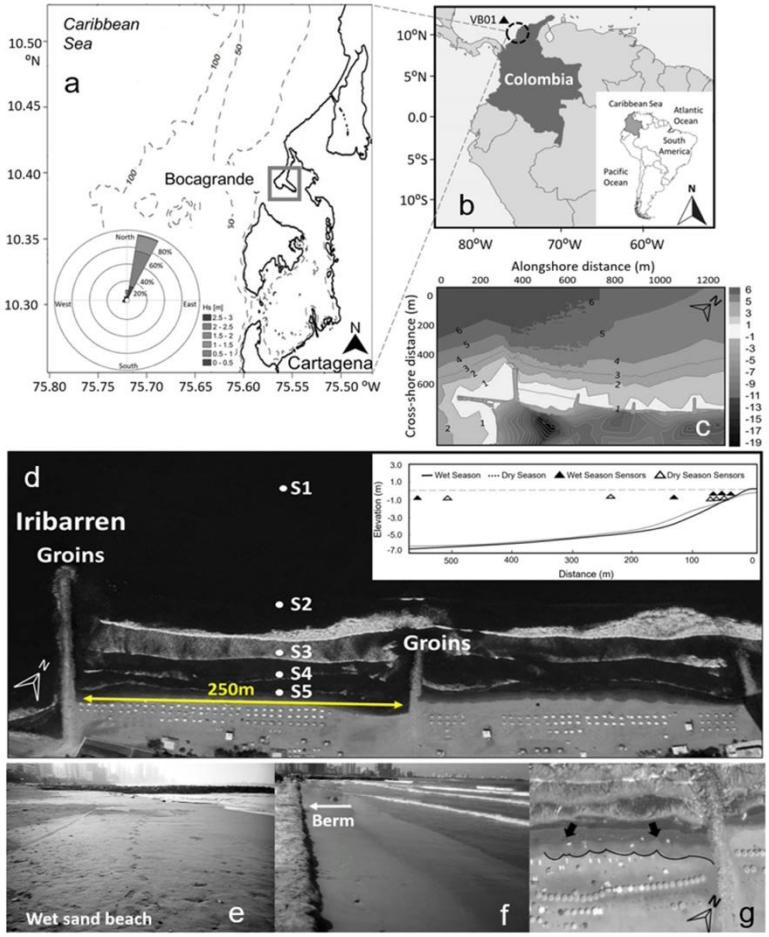

Figure 1. a) Location of Bocagrande in the Cartagena-Bolívar study area, Colombia, b) geographical location of virtual buoy VB01, c) bathymetry of Bocagrande Beach, color scale in meters (m), d) coastline in the dry and wet season, Bocagrande groins, and locations of instruments (S1, S2, S3 and S4), e) coastline in the dry season, f) coastline in the wet season, and g) *cusps*.

on the prevailing conditions. In addition to berms, *cusps* are evident in the area (Fig. 1g).

Field measurements

To study G and IG waves, instrumental data on swell hydrodynamic variables and current velocities were collected using pressure sensors and current meters. This work will follow the methods of Ruiz-Merchán et al. (2019).

During the field campaigns, which lasted four days each in the respective climatic seasons, hydrodynamic and morphological information was collected on Bocagrande Beach during the dry season in February 2015 and the wet season in November 2014.

To observe the evolution of G and IG swell and currents (u, v) as waves approach the coast, five *in situ* oceanographic device sets were deployed cross-shore, as shown in Figure 1d. Regarding sampling rate, the specific location, distance, and depth of each measuring equipment are shown (Table 1).

The sampling rate for the *in situ* Aquadopp Profiler devices (coordinate system X, Y) during the dry season was 1 Hz until a burst of 2,048 data points was completed, resulting in 34 min of record per hour. For the wet season, the sampling rate was 2 Hz until a burst of 1,024 data points was acquired, which lasted 17 min per hour. The only exception was the RBR instrument, which maintained a continuous record of 1 Hz in each survey (Fig. 1d). The choice of this sampling rate was made to achieve recording durations of 17 and 34 min, planned to confirm that these durations can produce a resolution suitable for G and IG wave frequencies. In this context, ideal recording times should range between

Table 1. Instrument configuration for pressure and current velocity measurements at Bocagrande Beach during wet and dry periods; sensors: S1: RBR pressure sensor; S2-S4: Aquadopp profilers; S5: Aquadopp HR.

Beach Bocagrande	Instruments	Sampling Regime		Distance (m)/Depth (m)		Variable	Location
		Wet period	Dry period	Wet period	Dry period		
	S1	1Hz Constant	1Hz Constant	650/6.3	504/5.9	Pressure	Mid water
	S2	2Hz 17 min h^{-1}	1Hz 34 min h^{-1}	107/4.2	232/2.5	Currents (u, v) and pressure	Shallow water
	S3	2Hz 17 min h^{-1}	1Hz 34 min h^{-1}	44/1.2	60/1.3	Currents (u, v) and pressure	Surf
	S4	2Hz 17 min h^{-1}	1Hz 34 min h^{-1}	26/0.6	52/0.7	Currents (u, v) and pressure	Surf
	S5	2Hz 17 min h^{-1}	1Hz 34 min h^{-1}	10/0.5	39/0.6	Currents (u, v) and pressure	Surf

17 and 34 min to ensure they are sufficiently long to obtain significant results (Haring et al. 1977, Aagaard & Greenwood 2008, Aucan & Ardhuin 2013, Morawski et al. 2018). Fifty sea states were obtained in each field campaign. In most consecutive sea states, energy was distributed in a similar but not identical manner, suggesting non-stationary behavior. The G and IG signals were filtered with a lower cut-off frequency of 0.05 Hz and an upper cut-off frequency of 0.5 Hz for the G waves. For IG waves, the lower cut-off frequency is 0.0033 Hz, and the upper cut-off frequency is 0.05 Hz. Subsequently, a Finite Impulse Response (FIR) band-pass filter was used (Conde-Frias et al. 2017a,b).

To assess the morphodynamic evolution of beaches, bathymetric measurements were conducted 24 h before the installation of monitoring equipment and the start of data collection. Surveys were conducted in the study area during each climatic season to assess hydrodynamic conditions in the surf zone under both calm (wet season) and high-energy (dry season) swell conditions. Bathymetry data were obtained with a single-beam echosounder (able to obtain depth for a single point only) with a spatial resolution of 1 m. A real-time differential GPS with geostationary satellite correction was used for the horizontal control of bathymetric data. In the sea area of the bay, a bathymetric survey was performed on an approximate area of 171.600 m^2.

Wave reanalysis

To analyze wave transformation from deep to shallow water and determine the morphodynamic state of Bocagrande Beach, three indicators were calculated: sediment fall velocity (w_s), the dimensionless velocity fall parameter (Ω), and the Iribarren number for deep-water (I_r) and shallow-water (I_{rb}) conditions (Stokes 1850, Iribarren & Nogales 1949, Wright & Short 1984, Ruiz-Merchán et al. 2019).

The Ω was calculated to assess sediment transport and define the morphodynamic state of the beach:

$$\Omega = \frac{H}{w_s T} \quad (1)$$

where H is wave height (m), T is the wave period (s), w_s is the sediment fall velocity (m s^{-1}), which was estimated using Stokes' law:

$$w_s = \frac{g(\rho_s - \rho)d^2}{18\mu} \quad (2)$$

where g is gravity (9.81 m s^{-2}), ρ_s and ρ are sediment and water densities, respectively (kg m^{-3}), d is the sediment grain diameter (m), and μ is the dynamic viscosity of water (Pas).

The Iribarren number was used to classify wave breaking:

$$I_r = \frac{m}{\sqrt{\frac{H_o}{L_o}}} \quad (3)$$

$$I_{rb} = \frac{m}{\sqrt{\frac{H_b}{L_o}}} \quad (4)$$

where m represents the beach slope ($\tan\beta$), H_o the deep-water wave height, H_b the breaking wave height, and L_o the deep-water wavelength.

To analyze the evolution of waves from deep water to shallow water through various processes, such as wave height and breaking, and to identify the predominant morphodynamic condition of the beach, the techniques of Ruiz-Merchán et al. (2019) were applied to collect wave series from the virtual buoy VB01 (Cartagena). Wave series were obtained from the virtual buoy VB01 (Cartagena), positioned at the

coordinates 11°N-74°W, sourced from the NOAA database, which utilizes the third-generation model WAVEWATCH III (WW3). This research considered the temporal changes in the data rather than presuming them to be constant or stationary. The 37-year dataset (from January 1979 to December 2016) was processed. Specifically, parameters such as significant wave height, maximum wave period, and average wave direction were examined. These reanalysis data were crucial for gaining insight into the modal state of the beach over the extensive 37-year period discussed.

The propagation of waves from deep waters was evaluated using Simulating Waves Nearshore (SWAN) (Booij et al. 1999), a third-generation wave model based on the action balance equation. It is widely used to simulate wave propagation in shallow waters, where the interaction between waves, seabed topography, and atmospheric conditions is complex and variable. The model was calibrated using the configuration proposed by Conde-Frias et al. (2017a) and Ruiz-Merchán et al. (2019). To integrate the model from deep waters to shallow waters, the significant wave height data measured by the pressure sensor (S1) located in intermediate waters during the two field campaigns conducted (the first during the dry season and the second during the wet season) were used. The reanalysis data is analyzed to calculate the deep-water Iribarren number (I_r). The SWAN model is used to propagate the Iribarren number at the foot of the beach to calculate the Iribarren number at break (I_{rb}). The quantification of the model's predictive capacity was performed by calculating the Willmott and Minkowycz bias index (Willmott et al. 1985). The Willmott index (d) measures the degree of agreement between predicted and observed values, ranging from 0 (no agreement) to 1 (perfect agreement). In contrast, the Bias index evaluates the average systematic error, with values close to 0 indicating little bias, positive values reflecting overestimation, and negative values underestimation. These indices together provide important context for assessing the reliability of the results.

The wave series propagated from the geographical point of VB01 (Fig. 1b) to the location of the RBR(S1) sensors (Fig. 1d). The RBR location points coincide with the seaward boundaries of detailed bathymetries of the beach. The above is based on a SWAN computational domain consisting of 462 nodes in the x-direction and 570 nodes in the y-direction, with a cell resolution size of 200 m.

After analyzing significant wave height and peak period, the beach morphodynamic state is determined using Ω and wave breaking characteristics, assessed with I_r and I_{rb}. This approach, developed by Iribarren & Nogales (1949), helps understand the dynamic balance of beach sediments and how they respond to wave action (Ruiz-Merchán et al. 2019).

Cross wavelet transform (wavelets XWT) and wavelet coherence (WTC)

The wavelet method is a powerful tool for interpreting changes observed in the surf zone, identifying the time-frequency domain of non-stationary signals, and analyzing them separately (Ruiz-Merchán et al. 2019).

Wavelet analysis generated a series of results that revealed the energy processes associated with the transformation of waves as they move from offshore to the coast, allowing for the classification of the types of IG waves reaching the beaches of Bocagrande during different climatic periods. By using the XWT and the WTC, it is possible to evaluate the correlation between the two variables that vary with different frequency scales, which means that it is possible to identify if there is a significant correlation between the η and current velocities (u and v) at specific time and frequency scales, thus identifying the patterns of IG waves.

Wavelet-based techniques were applied to analyze G and IG processes in the surf zone of Bocagrande Beach. CWT decomposed η and current velocities (u, v) into the time-frequency domain, showing transient oscillatory patterns. XWT quantified common power and phase relationships, and WTC measured the normalized association across scales (where 0 indicates no correlation and 1 indicates perfect synchronization). Statistical significance was evaluated using Monte Carlo simulations with 1,000 surrogate series under a red-noise null hypothesis at 95% confidence level, distinguishing genuine hydrodynamic interactions from spurious correlations (Grinsted et al. 2004, Ruiz-Merchán et al. 2019).

For stationary, cross-shore, and alongshore progressive waves (including progressive edge waves), the phase lag between velocities u and v (as well as velocity u and η) is 90°. In contrast, for velocities u and v stationary waves (including edge waves), the phase lag is 0 or +180° between velocities u and v (or velocity u and η, respectively) (Huntley & Bowen 1973). The phase lag between velocity v and η is 0° for alongshore progressive waves and +90° for alongshore standing waves. In the presence of alongshore standing waves, η and velocity v are 0 or +180°.

Cross-wavelet spectral analysis enables the determination of the correlation between two time series as a

function of frequency, representing the areas of common energy between two time series, as well as the phase difference between the variables (Grinsted et al. 2004). Furthermore, as proposed by Winter et al. (2017) and Ruiz-Merchán et al. (2019), it is possible to classify the type of IG wave present on the beach, since when analyzing the phase relationship between η and the alongshore and cross-shore velocities, a lag will be found for each pairing (η-u), (η-v), and (u-v), allowing us to identify the type of IG acting in the surf zone.

RESULTS

The significant wave height (*Hs*) and the relative peak period (*Tp*) values for the SWAN model and data recorded by the S1 sensor in Bocagrande Beach, both for dry and wet seasons (Figs. 2a-d).

The Willmott index revealed a correlation coefficient of 0.9 for *Hs* and 0.4 for *Tp* between *in situ* data and modeled data. Despite the low Willmott index for *Tp* and the limitations of wave reanalysis databases in representing *Tp*, the bias indicated that the model underestimated *Hs* by 5% and *Tp* by 3%. It is thus worth highlighting that the model accurately presents the variation of *Tp* (Figs. 2c-d). Conversely, Hs histograms for wet and dry seasons in Bocagrande, plotted from SWAN model results at the location of sensor S1 (Figs. 2e-f), indicated that *in situ* measurements were typical of the climate in the study area for both seasons.

The prevailing direction of swell incident on the study area was NW (322 to 328° azimuth). According to shallow and deep-water values at Iribarren, obtained from WWIII, and *Hs* and *Tp* series propagated with the SWAN calibrated model (Figs. 3a-b), swell in shallow waters is mostly comprised of spilling breakers progressively dissipating swell energy along the profile. However, *plunging* breakers may also occur sporadically. In addition, Ω for this beach equals 4.40 for the dry season and 4.02 for the wet season.

Following Wright & Short (1984), the values mentioned above correspond to a dissipative-intermediate beach of cross-shore bar and rip type. That is, the beach is characterized by having one or several longitudinal bars parallel to the coastline and separated by troughs, a nearly uniform alongshore morphology, and a significant run-up reach. It is worth noting that, according to previous studies (Guza & Inman 1975, Pruszak et al. 2007), the presence of an irregular seabed enables subharmonic edge waves to act in the shoreline zone, contributing to the generation of cusps and the occurrence of weak rips.

The Fourier spectra for the η series corresponding to dry and wet seasons is shown (Fig. 4). Throughout the dry season, sensor S2 recorded a concentration of energy in the G regime (8 s period) in all sea states. Simultaneously, a low contribution of IG energy was verified. Given that this sensor was located before the shoaling zone, the pattern mentioned above may imply the presence of IG waves reflected off this type of beach. That is, sensor S2 was placed before the shoaling zone, and waves at this point did not shoal or break. Consequently, the energy recorded by this sensor should be of the G regime, with little detection of IG oscillations. As a result, the presence of IG energy in this sensor may be attributed to the presence of leaky waves.

Sensor S3 recorded two prevailing energies: one in the G regime (8 s period) and another in the IG regime (111 s period). The IG regime energy increased in comparison to that of sensor S2. These records are consistent, as sensor S3 was located close to the shore. Even though part of the energy was concentrated on the G band (Fig. 4b), as a swell reaches shallow water near the coast, the wave slows down due to the shallower depths, causing the top to topple over and break. This breaking process releases a portion of the wave's energy into other frequencies, including the low-frequency in the surf zone. The IG wave increases its energy because it is not associated with a group of waves that transfer energy from G to IG frequencies (Longuet-Higgins & Stewart 1962). Likewise, an increase in IG energy at sensor S3 can be related to edge waves in the surf zone (Oltman-Shay & Guza 1985).

Regarding the results of the wet season, these revealed a swell with less energy compared to that in the dry season. In fact, the prevailing energy recorded was in the G band, surrounding the 8 s period in sensors S2, S3, and S4. Because of this, energy spread to other frequencies could be observed in sensors S3 and S4 (Figs. 4d-e), which is consistent with the location of these sensors in the surf zone, where IG energy is significant.

Power density spectra of current velocities (u and v) for dry and wet seasons are shown (Fig. 5). In this case, energy spectra u are higher in the dry season compared to the wet season (Figs. 5a-e). Regarding this difference, energy spectra for velocity u are more significant than the energy of velocity v (Figs. 5a-b, f-g). Between sensors S2 and S3, the prevailing energy observed for u was approximately 8 s in the G regime (Figs. 5a-b).

It is worth highlighting that little energy spread was observed in the lowest frequencies of the spectrum, with

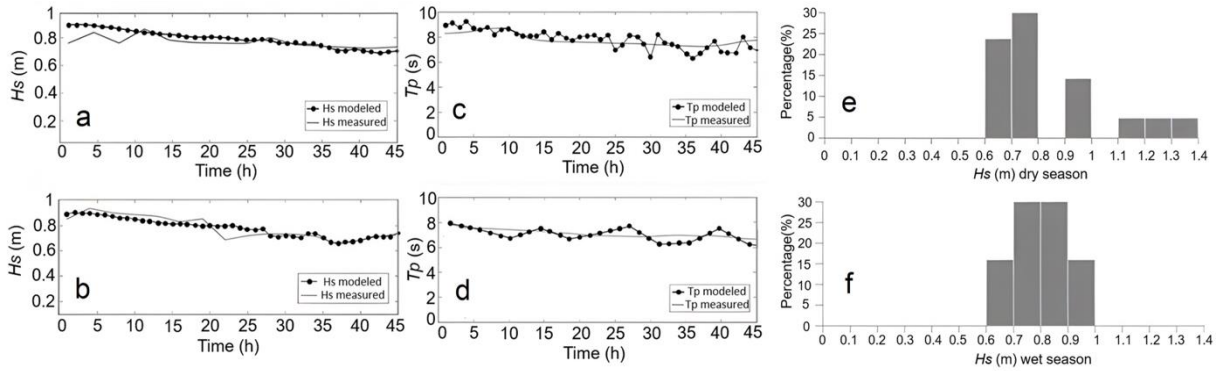

Figure 2. Results of the calibrated SWAN model and *Hs* histograms for Bocagrande Beach: a, c, e) dry season, and b, d, f) wet season. *Hs*: significant wave height, *Tp*: the relative peak period.

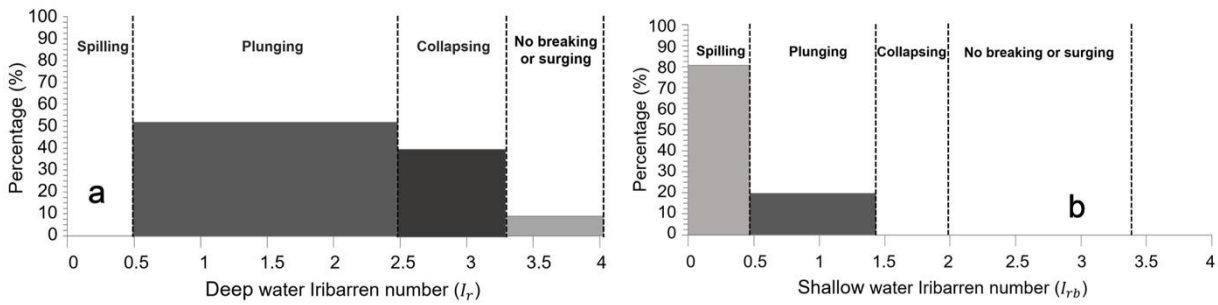

Figure 3. Percentage of various types of waves breaking on Bocagrande Beach: a) I_r in deep waters, and b) I_{rb} in shallow water.

a significant G band remaining in sensor S3. Regarding the velocity v spectra (Figs. 5f-g), high-frequency energy prevailed in sensor S2, whereas sensor S3 exhibited energy restricted to low frequencies. Likewise, energy transfer was evident in sensor S3, resulting in a significant contribution of G waves to this component of currents. In the same way, IG energy increased as the swell approached the coast.

Energy spectra for current velocities (*u* and *v*) revealed lower energy levels in the wet season compared to the dry season. During the wet season, the velocity component *u*, recorded by sensors S2, S3, and S4, concentrated on the G band around the 8 s, whereas the IG band energy was recorded by sensors S3 and S4. In the case of velocity component *v*, the energy G recorded by sensor S2 was less than that of sensors S3 and S4. Lastly, in sensor S3, the perceived energy G focused around 8 s, evidencing a low contribution of the IG band. In contrast, sensor S4 recorded the spread of G and IG energies, with the IG band prevailing in the spectrum.

Spectral analysis of waves by CWT

The energy behavior of G and IG was similar to that shown in the Fourier spectra plots. In this study, Hmo, or significant wave height, represents the average height of the highest one-third of waves recorded during a specific time period. It is a widely used parameter to characterize the typical wave size and energy in marine environments. Tp, or peak period, is the time interval between consecutive crests of the dominant waves, reflecting the main frequency of the wave energy. Together, Hmo and Tp provide essential information about the intensity and characteristics of the sea state, with higher values indicating larger and longer-period waves, as observed during the wet season.

The CWT results in this section reveal variations in G and IG energy associated with weather conditions. According to sea weather results of sensor S1, the greatest sea state energy was Hmo = 0.36 m and Tp = 8.0 s in the wet season, and Hmo = 0.75 m and Tp = 9.0 s for the dry season.

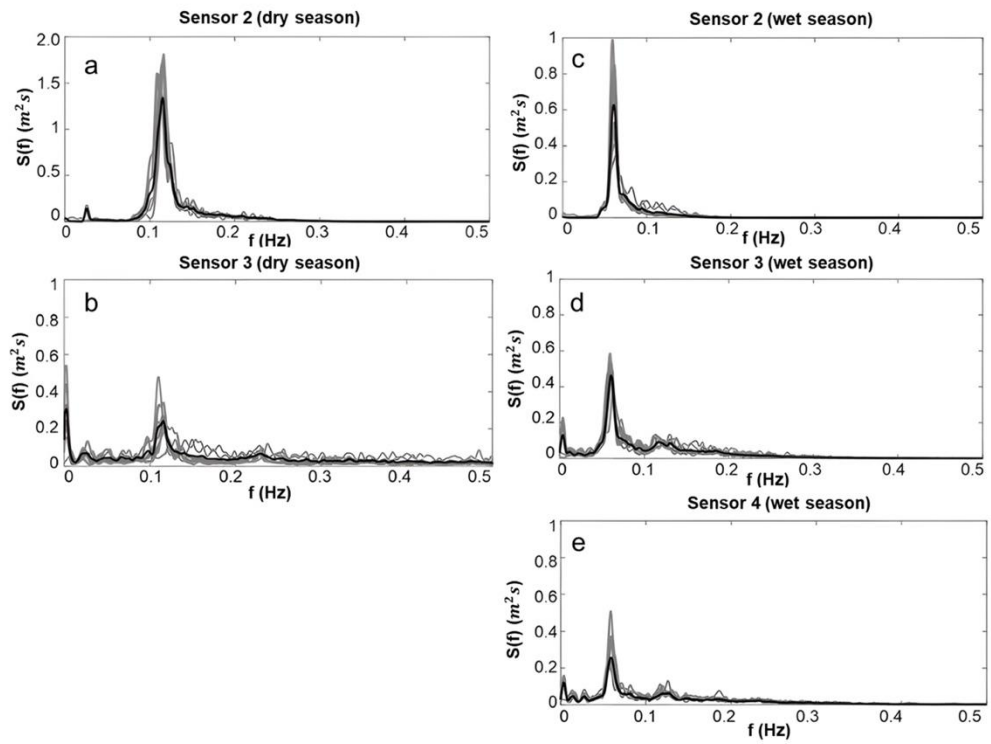

Figure 4. Free surface elevation (η) spectra for all sea states recorded at Bocagrande Beach by the sensors: a-b) S2 and S3 dry season; c-e) S2, S3, and S4 wet season. The black line corresponds to the average spectrum of all sea states. The vertical axis shows the spectral density, S(f) (m^2 s), and the horizontal axis represents frequency, f(Hz), where f denotes wave frequency.

Figure 6 shows the η spectrum for the dry and wet seasons. In this case, G energy was dominant, due to the high significance of G energy occurrence, which was concentrated in the 8 s period and remained constant throughout. In the dry season, IG energy was recorded as discontinuously distributed over the 64-512 s periods, with moderate significance. Regarding the wet season, a smaller IG signal was observed, with low significance across the entire time domain.

Figure 7 shows the evolution of η, u, and v, recorded by sensors S2 and S3 during the dry season. According to sensor S2, G energy is statistically significant, with periods ranging around 8 s through the study interval in the η, u, and v spectra. Parallel to these, the occurrence of IG signals is shown, concentrated in periods of 32-256 s in the η, u, and v spectra, with moderate significance for intermittent signals between the 400 and 1,600 s intervals. Regarding sensor S3, the η spectra revealed a significant G-band energy, concentrated in periods of approximately 8 s. In addition, some important discontinuous IG contributions were observed for periods between 64 and 256 s, specifically in intervals 400-1,000 and 1,600-1,800 s. On the other side, the oscillation of the G regime remains significant. In addition, an IG signal was observed, with high significance in periods exceeding 64 s and intervals ranging from 400 to 1,800 s. Regarding velocity v, the G energy obtained is of low significance, whereas the IG signal made significant contributions in the periods between 128 and 256 s and in the 200-400 and 800-1,600 s intervals. In addition, the velocity components (u and v) exhibited high significance values of the IG signal in periods between 64 and 256 s.

Figure 8 shows the evolution of η, u, and v, recorded during the wet season by sensors S2, S3, and S4. Sensor S2, located before the surf zone, showed that the G signal was prevailing and significant in η and u for the 8 s period, which occurred throughout the entire sea state. The IG oscillations were distributed in different periods, presenting discontinuous energy signals with moderate significance. The IG signal for velocity v was prevailing, continuous, and highly significant in the 128-256 s band (Fig. 8c), although it was discontinuous in the interval 1,000-1,200 s as it exhibited signal loss. On the other side, the energy record of sensor S3 re-

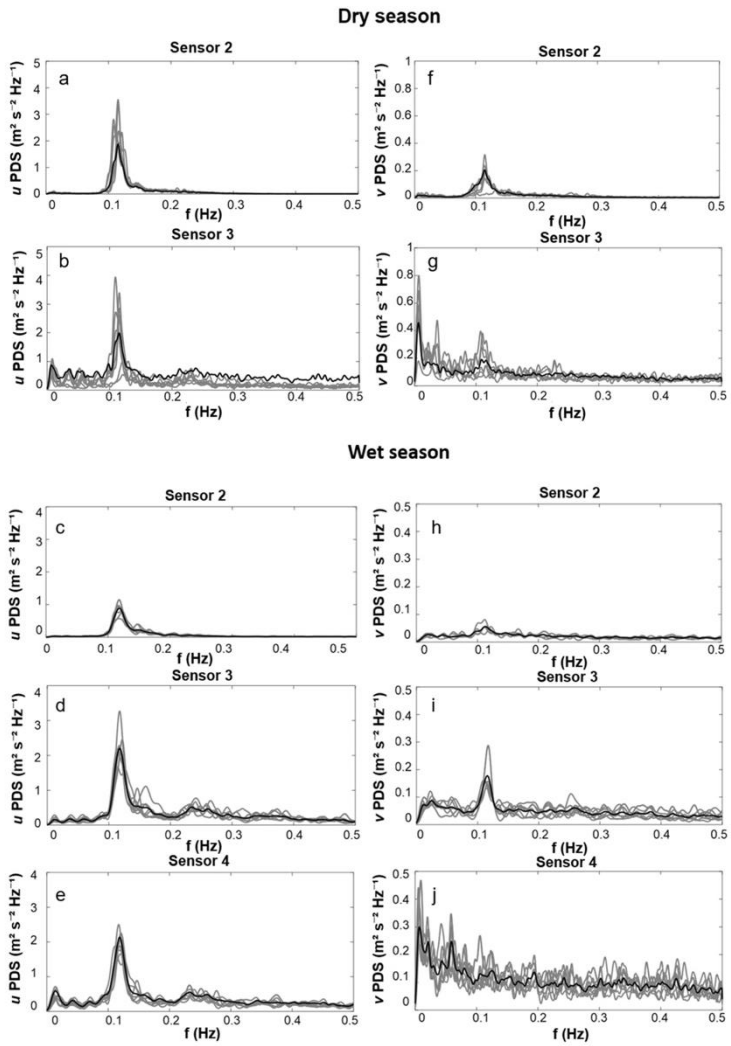

Figure 5. Spectra of cross-shore (*u*) and alongshore (*v*) velocity spectra for all sea states recorded (gray lines) by sensors at Bocagrande Beach during the wet and dry seasons: a-b, f-g) represent the dry season c-e, h-j) represent the wet season. Gray lines show the power spectral density (PSD) of each individual sea state, and the black line represents the average spectrum across all sea states. The PSD, plotted as a function of frequency (*f*), represents the energy distribution (in $m^2 s^{-2} Hz^{-1}$) of the instantaneous velocity components *u* (cross-shore) and *v* (alongshore).

vealed a more transcending IG signal compared to sensor S2 (Fig. 8e).

According to the values of η and u from sensor S3, oscillations were detected in the continuous G band at 8-s periods, with high magnitudes. IG regime signals with moderate to high significance were also detected in the 32-256 s. Nevertheless, the IG signal in η was absent in the 64-256 s periods corresponding to time intervals 500-700 s, as well as in velocity *u* in periods 64-128 s within the time interval 200-300 s. For the case of velocity *v* (Fig. 8f), a maximum of IG energy was evidenced for the 64-256 s period, with discontinuous magnitudes in the time interval 700-800 s. Data from sensor S4 displayed a high significance in the IG regime, which prevailed in periods between 64 and 256 s, particularly within the 200-800 s interval. They were more pronounced for *v*. For the cases of η and u, both G and IG signals were important. However, they were intermittent as indicated by the CWT spectra.

Cross-correlation and coherence analysis (XWT and WTC)

Wavelet, XWT, and WTC tools are used to identify common power levels and relative phases in the frequency-space-time of parameters η, *u*, and *v*, particularly for high-tide and low-tide sea states. It

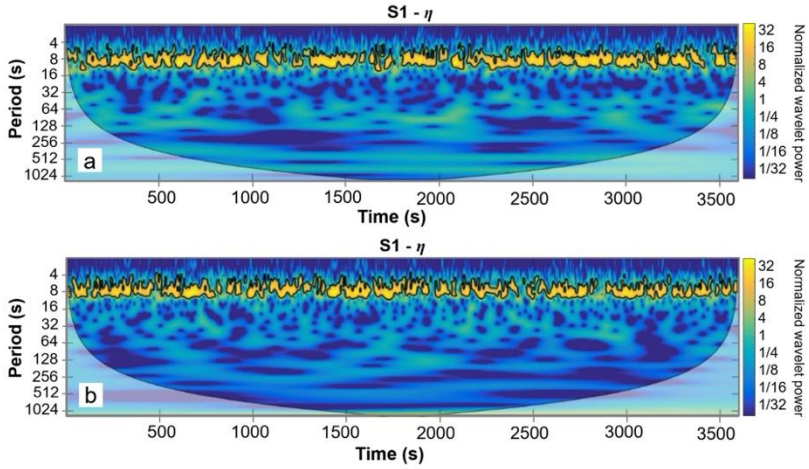

Figure 6. Wavelet spectra of free surface elevation (η) recorded at Bocagrande Beach by sensor S1 during the a) dry season (Hmo = 0.75 m, and *Tp* = 9.0 s), and b) the wet season (Hmo = 0.36 m, and *Tp* = 8.0 s). *Tp*: the relative peak period.

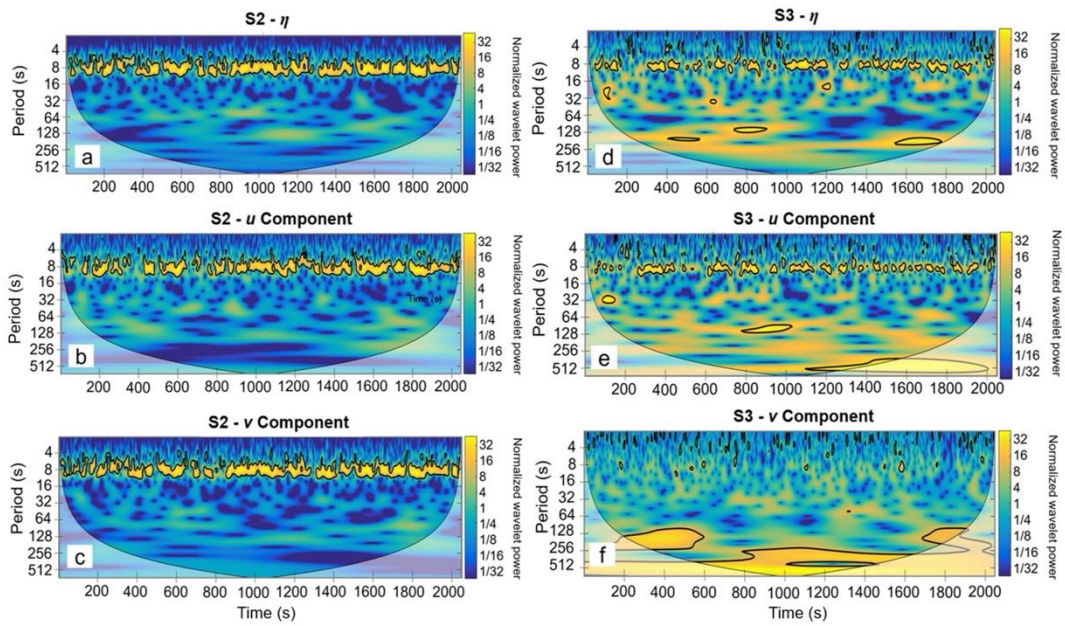

Figure 7. Wavelet spectra of free surface elevation (η) and velocity components at Bocagrande Beach during the dry season (Hmo = 0.75 m, *Tp* = 9.0 s): a) η at S2, b) cross-shore velocity (u) at S2, c) alongshore velocity (v) at S2, d) η at S3, e) cross-shore velocity (u) at S3, and f) alongshore velocity (v) at S3. *Tp*: the relative peak period.

allows for observing the effect of tides and analyzing the influence of G and IG energy as the tide range increases or decreases in the study area.

According to Figure 9, sensor S2 recorded an IG signal with high significance. XWT and WTC spectra revealed that the relationship between η and u presented a moderate correlation and a very significant coherence for the period band between 64 and 256 s within the 800-1,000 s time interval. The phase angle between η and u was 90°, indicating that η led u. At the same time, a moderate correlation was found between η and v, as well as a highly significant coherence in the periods between 128 and 256 s, within time intervals of 400-800 and 1,400-1,600 s. Both variables are out of phase by 90°, implying that η leads v. Regarding XWT and WTC between η and u in sensor S2, the highest significance values were found in the IG band between 64 and 128 s, as well as in the intervals of 1,600-1,800 s. The phase angle was 0°, showing that u and v are moving in the same direction.

For sensor S3 (Fig. 10), the greatest correlation and coherence values for both η-u and η-v relationships were found for periods between 32 and 256 s, corresponding to time intervals of 600-1,400 s. In this

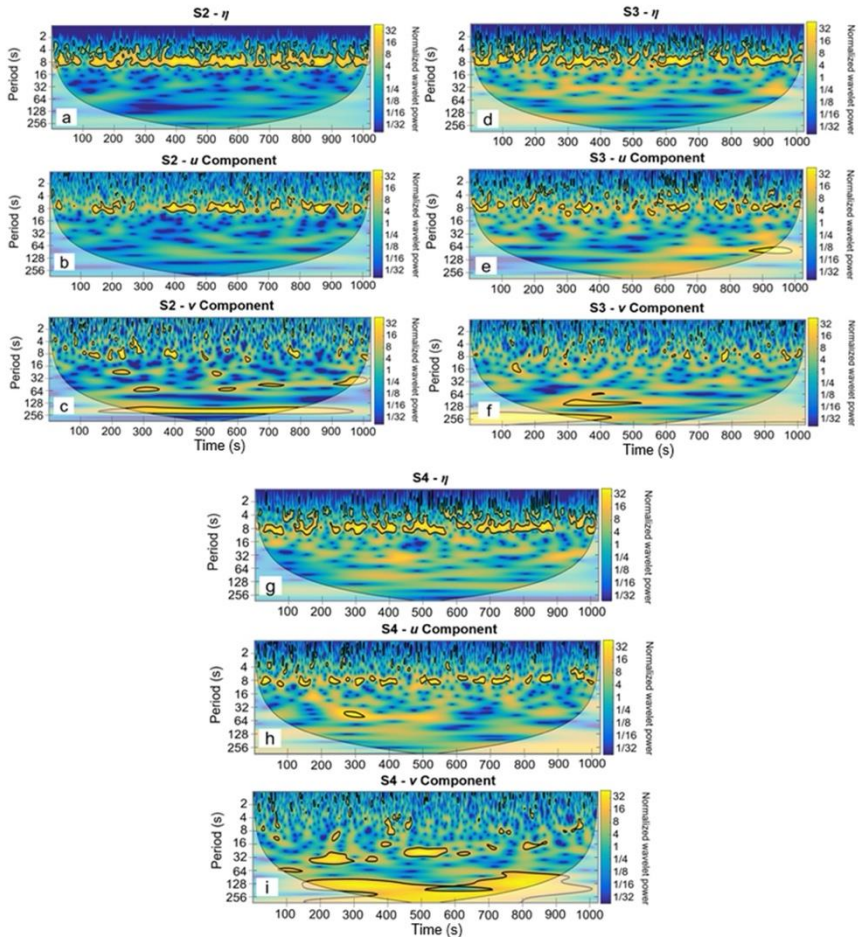

Figure 8. Wavelet spectra of free surface elevation (η) and velocity components at Bocagrande Beach during the wet season (Hmo = 0.36 m, Tp = 8.0 s): a) η at S2, b) cross-shore velocity (u) at S2, c) alongshore velocity (v) at S2, d) η at S3, e) velocity u at S3, f) velocity v at S3, g) η at S4, h) velocity u at S4, and i) velocity v at S4.

case, IG prevailed, with a phase angle of 90° and η leading. On the contrary, the XWT and WTC plots of u-v showed both variables in phase for periods 64-256 s within time intervals 400-1,000 and 1,600-1,800 s.

The values of variables η, u, and v recorded by sensor S2 reveal that, in the XWT and WTC spectra, the strongest relationship was between η and u (Figs. 11-12). This relationship was particularly strong in periods around 8 s, displaying high significance throughout the entire time interval, with a phase angle of 0°. The latter implied that η and u were in phase, with a prevalence of the G regime in the spectrum. Regarding the IG signal, it was visible in periods close to 64 s and in the interval of 100-300 s. In terms of the relationships η-v and η-u, the energy relationship between variables was not significant and very discontinuous.

The analysis of the wavelet spectrum for selected sea states revealed that, for sensor S2, placed in the shoaling zone, G energy dominated the spectrum, whereas IG energy was low.

In sensor S3, the correlation and coherence η-u spectra evidenced that G energy was concentrated around 8 s periods, showing a strong relationship between variables and high significance throughout the entire time interval. However, an IG signal was observed in 32- and 128-s periods, corresponding to the 100-400 s interval. These featured a phase angle of 0°, indicating that both variables are in phase with high covariance values. In terms of the η-v relationship, G energy was discontinuous in periods close to 8 s. Likewise, IG energy was located within the 128 s period band, spanning the 700-900 s time interval, with a phase angle of 0° and high covariance values.

XWT and WTC spectra for the u-v relationship revealed that G energy was highly dissipated, as it was not as well represented as in the η-u spectrum. In turn, a high significance of IG energy was observed in the

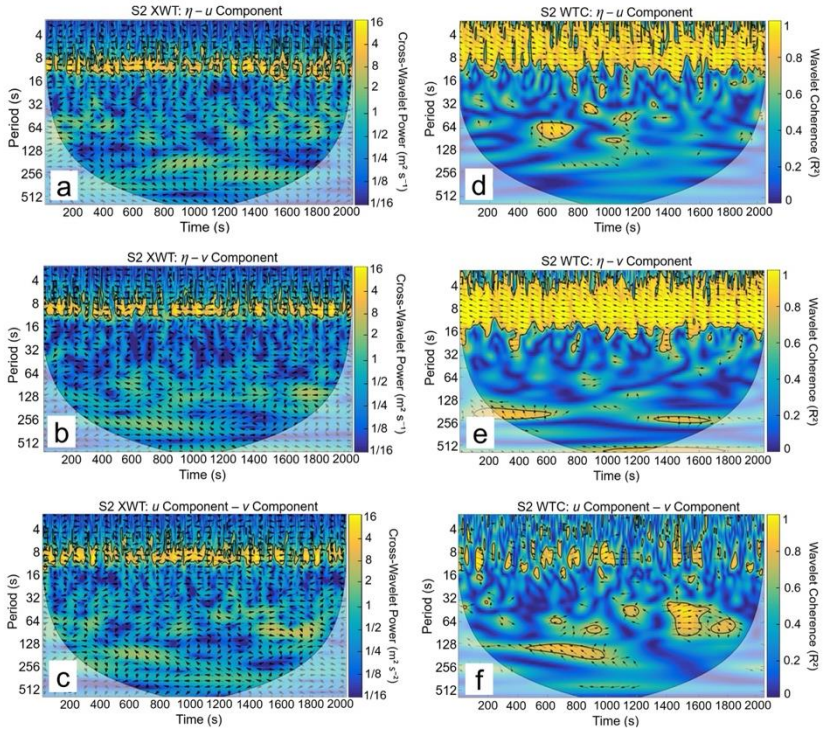

Figure 9. Cross-wavelet transform (XWT) and wavelet coherence (WTC) spectra at Bocagrande Beach during the dry season at sensor S2. a) XWT between η and u, b) XWT between η and v, c) XWT between u and v, d) WTC between η and u, e) WTC between η and v, and f) WTC between u and v.

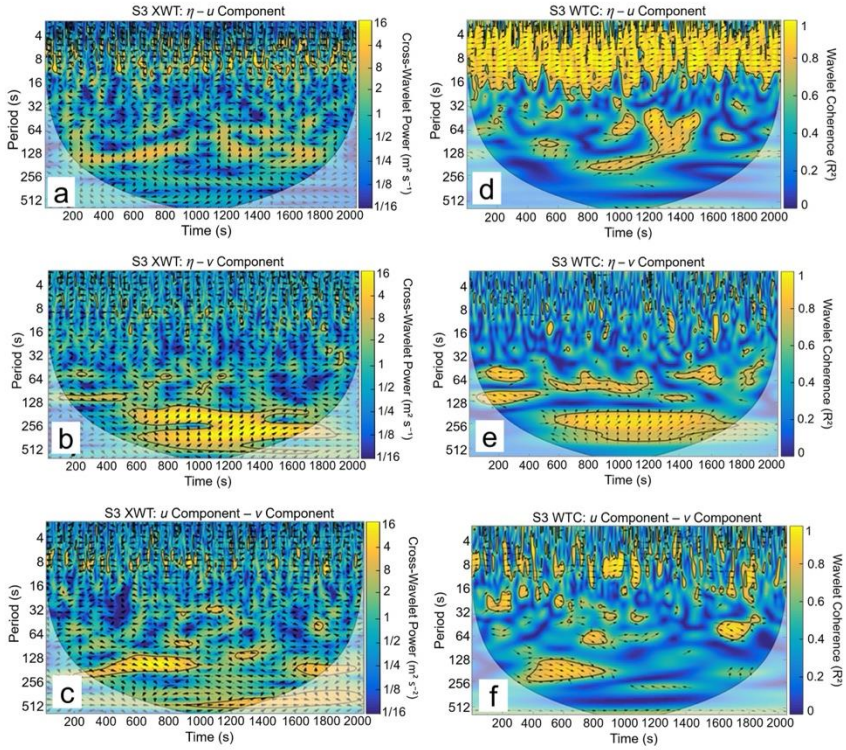

Figure 10. Cross-wavelet transform (XWT) and wavelet coherence (WTC) spectra at Bocagrande Beach during the dry season at sensor S3. a) XWT between η and u, b) XWT between η and v, c) XWT between u and v, d) WTC between η and u, e) WTC between η and v, and f) WTC between u and v.

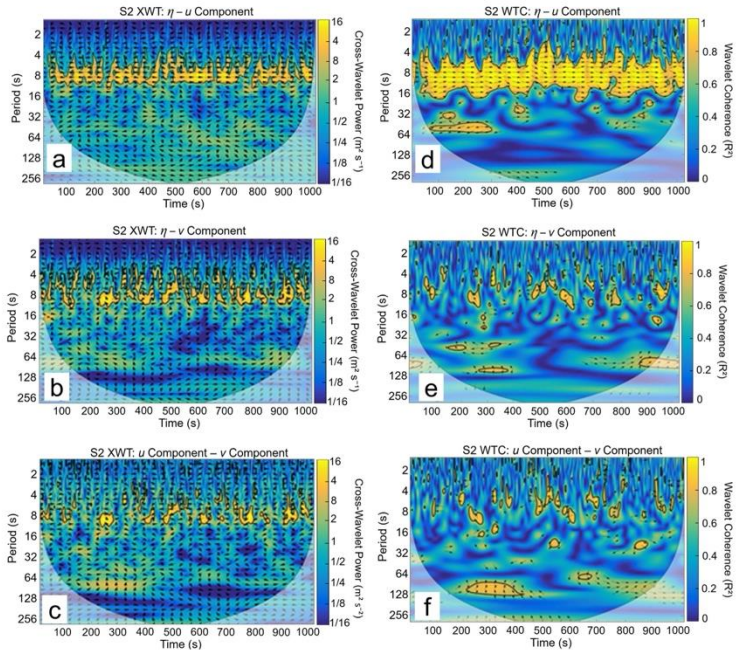

Figure 11. Cross-wavelet transform (XWT) and wavelet coherence (WTC) spectra at Bocagrande Beach during the wet season at sensor S2. a) XWT between η and u, b) XWT between η and v, c) XWT between u and v, d) WTC between η and u, e) WTC between η and v, and f) WTC between u and v.

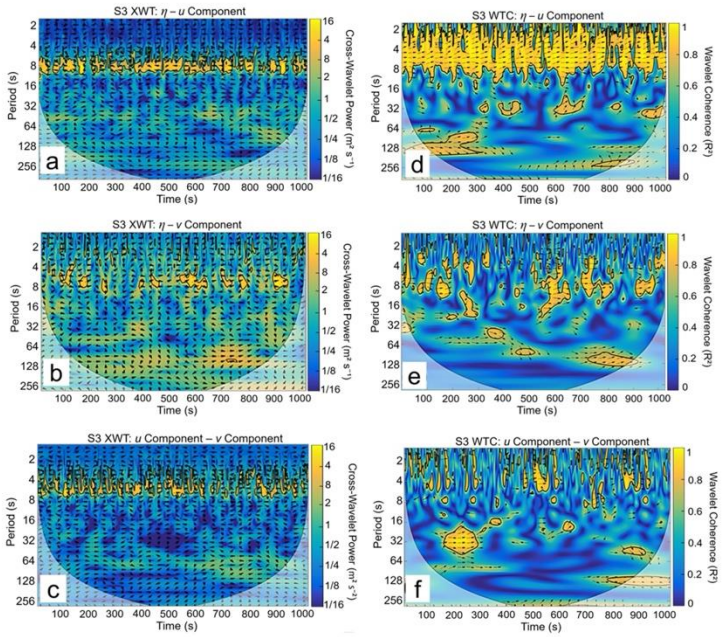

Figure 12. Cross-wavelet transform (XWT) and wavelet coherence (WTC) spectra at Bocagrande Beach during the wet season at sensor S3. a) XWT between η and u, b) XWT between η and v, c) XWT between u and v, d) WTC between η and u, e) WTC between η and v, and f) WTC between u and v.

band between 32 and 64 s, in the 200-300 s interval. In this case, a phase angle of 0° indicates that variables were in phase, with coherence values close to 1. It is worth highlighting that, in sensor S3, signals for v currents and the IG regime gained more importance, whereas G energy decreased, as this sensor was located in the surf zone. Because of this, spectra related to the velocity component v (Figs. 12 b-c, e-f) featured greater

energy levels at this point of the beach, as the swell released energy during breaking. In this process, G energy was dissipated, and IG became more important, as confirmed by energy spectra, which revealed the strong relationships between η-u, η-v, and u-v. Additionally, coherence values close to 1 were observed, indicating a strong correlation between the signals. In fact, the same trend, although with less energy, was evidenced in S4 (Fig. 13), perhaps due to the dissipation of G energy at this point, caused by turbulence and friction with the sea bottom, among other factors.

Global wavelet spectrum analysis

Figures 14 and 15 show the global wavelet spectra for selected sea states in the dry and wet seasons. During the dry season, the observed contribution of the IG signal for velocities u and v was more evident for sensor S3, which was located closer to the beach. Nevertheless, velocity v displayed a greater IG energy compared to velocity u (Figs. 14d,f).

Regarding the wet season, the G signal was highly significant, as it was above the 95% confidence interval line, implying that energy in the G range prevailed more frequently during the wet season. For the same reason, when G waves were present, it was difficult for global wavelet spectral analysis (Fig. 15a) to feature IG waves above the significance threshold. However, this does not mean that the IG signal was non-existent or unimportant; rather, it was far stronger due to its higher occurrence rates and greater power.

DISCUSSION

This section presents the analysis of pressure and velocity (u and v) measurements taken at Bocagrande Beach in Cartagena, Colombia, during both the dry and wet seasons. It examines the mechanisms of the IG wave energy propagation and the transformation of the G wave energy as waves approach the shoreline. The study also explores the relationship between G and IG energy, the behavior of current velocities in the surf zone, and the distinctive IG energy patterns observed in the area. These factors are key to understanding the complex dynamics of wave-seabed interactions in the coastal zone.

The parameters Ω, I_r, and I_{rb} provide valuable support for the analysis of results, as they help identify bar morphology and beach type (Masselink & Pattiaratchi 2001). According to Wright & Short (1984), the Iribarren number -also known as the breaker parameter- indicates that Bocagrande Beach can be classified morphologically as a dissipative-intermediate beach with alongshore bar and rip characteristics. The study site exhibits a strong rhythmic circulation pattern that weakens near the shoreline. Weak rip currents and pronounced beach *cusps* are also observed, influenced by variations in beach slope ($0.003 < \tan \beta < 0.018$). These slope variations contribute to *cusp* formation, as IG energy is not fully dissipated (Vidal et al. 1995). Montaño-Muñoz et al. (2018) reported that IG energy dominates the spectrum at sensors located closest to the shore at Bocagrande Beach. Similarly, Conde-Frias et al. (2017b) found that IG energy is the primary driver of swash zone dynamics on this dissipative beach.

Fourier and wavelet analyses identified the main energy modes -G and IG- that contribute to the formation of circulatory systems in different zones of Bocagrande Beach. The results show that as waves approach the shore, energy in the G band decreases due to bottom friction and wave breaking, while IG energy increases near the shoreline. Additionally, the energy of the velocity components (u, v) was significantly higher during the dry season than in the wet season, according to the Fourier spectral analysis, which aligns with the findings of Otero et al. (2016), who describe two distinct seasonal patterns: the dry season, characterized by stronger winds, lower precipitation, and more intense swell; and the wet season, with weaker winds, higher precipitation, and weaker surf. Furthermore, the global wave analysis confirmed the dominant frequencies identified in the Fourier analysis.

Wavelet spectrum analysis during the dry season in Bocagrande (Figs. 6-7) showed that G energy dominated at the sensor farthest from the coast (S1), while IG energy remained at moderate levels. These findings align with those of Conde-Frias et al. (2017b) and Baldock (2012), who noted that wave energy is not fully dissipated, with a portion being reflected. Although reflection is typically minimal on dissipative-intermediate beaches, characterized by spilling breakers, it still plays a significant role in surf zone hydrodynamics. Specifically, rip currents influence both the breaking and the formation of standing waves. In contrast, during the wet season, energy evolution analysis revealed that swell G energy decreased as it moved shoreward. IG energy became dominant in the surf and swash zones due to increased wave height nearshore, driven by shoaling and the transfer of energy from G waves. The increase in IG energy was more pronounced than the reduction in G energy, suggesting that the sensors also captured IG energy generated through reflection processes. This energy transfer mecha-

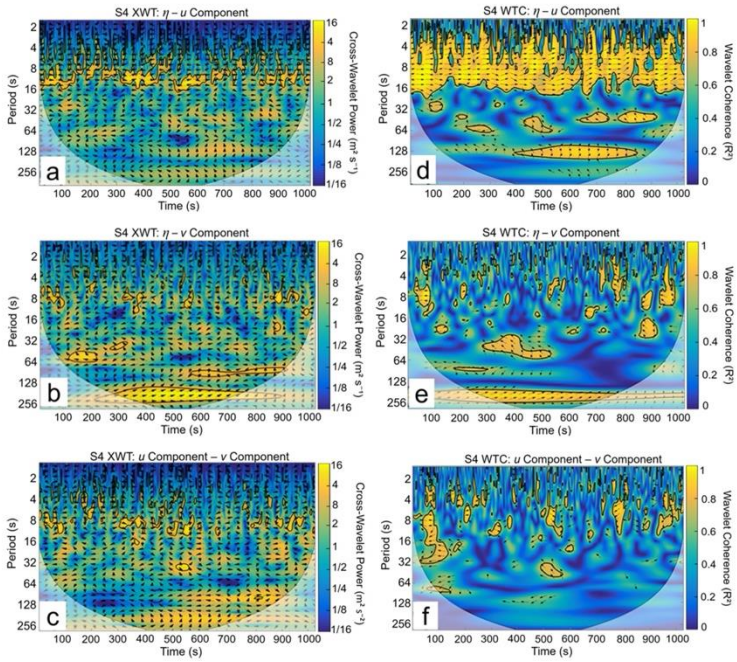

Figure 13. Cross-wavelet transform (XWT) and wavelet coherence (WTC) spectra at Bocagrande Beach during the wet season at sensor S4. a) XWT between η and u, b) XWT between η and v, c) XWT between u and v, d) WTC between η and u, e) WTC between η and v, and f) WTC between u and v.

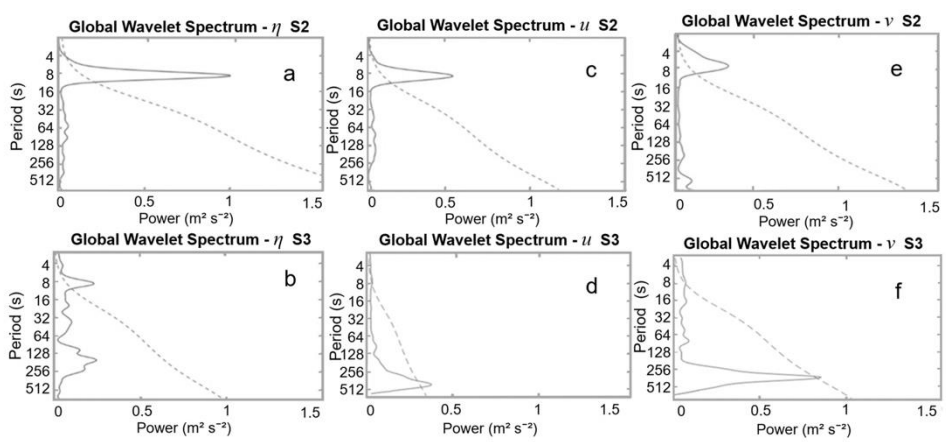

Figure 14. Global spectra of free surface elevation (η) and cross-shore (u) and alongshore (v) velocities measured by the sensors during the dry season at Bocagrande Beach. a-b) η measured by sensors S2 and S3, respectively; c-d) u component from the same sensors; and e-f) v component. The y-axis represents the period in seconds, and the x-axis represents spectral power in units of m^2 s^{-2}. The solid line indicates the observed power, and the dashed line represents the statistical significance threshold. Peaks in power reveal the dominant temporal scales of variability at each sensor.

nism, as swell approaches the coast, was previously observed at the same site by Montaño-Muñoz (2015), who attributed these changes to linear energy transfer processes.

The results from sensors S2, S3, and S4, located in the surf zone of Bocagrande Beach, were similar to those reported for Costa Verde (Ruiz-Merchán et al. 2019), despite the differing morphological settings of the two beaches. In both cases, it was confirmed that as swell approaches the coast, G energy decreases, though it remains dominant in the spectral range around 8 s for both η and the velocity component v. However, a slight influence of IG energy was observed in the u component. Similar to the dry season, IG energy dominated the spectrum of the v velocity component. This observation aligns with previous studies (Huntley

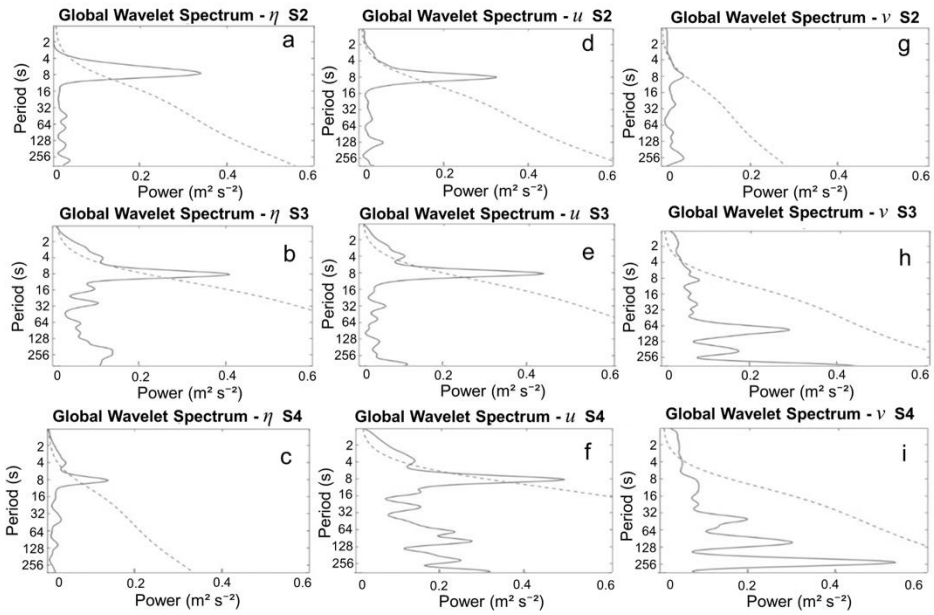

Figure 15. Global spectra of free surface elevation (η) and cross-shore (u) and alongshore (v) velocities obtained from the sensors deployed during the wet season at Bocagrande Beach. a-c) η measured by sensors S2, S3, and S4, respectively; d-f) u component from the same sensors; and g-i) v component. The y-axis represents the temporal scale in days, and the x-axis represents spectral power in units of $m^2 s^{-2}$. The solid line indicates the observed power, and the dashed line represents the statistical significance threshold. Power peaks highlight the dominant temporal scales in the local hydrodynamic variability.

et al. 1981, Oltman-Shay & Guza 1985), which confirmed the presence of IG energy in the v component near the shoreline. Moreover, studies by Coco et al. (2003, 2004) demonstrated that strong v currents can contribute to the dissipation of beach *cusps*. It is important to note that v currents are influenced not only by wave breaking but also by local coastal features, such as groins and other human interventions along the shoreline.

On the other hand, the behavior observed in XWT and WTC spectra (Figs. 9-10) during the dry season at Bocagrande Beach suggests the presence of leaking and edge waves, both cross-shore and alongshore. The 90° phase angle between η (sea level elevation) and velocities (u and v) indicates that waves were in a standing state due to the reflection of 50% of the swell incident on the beach. This dynamic is consistent with previous findings (Montaño-Muñoz 2015, Ruiz-Merchán et al. 2019), which also document the impact of reflection on swell behavior. These results are essential to understanding the hydrodynamic behavior in these coastal areas, particularly in terms of their interaction with beach morphology (Cueto et al. 2022). The results obtained in Bocagrande support the hypothesis of edge wave occurrence, as mentioned by the analysis of Montaño-Muñoz et al. (2018). The location of the beach, situated between two groins, may be enhancing the capture of part of the energy generated by these waves. These findings are also consistent with the work of Austin & Masselink (2006), which indicates that, in the case of standing edge waves, a 90 or -90° phase difference is expected between η and current velocities (u and v), whereas currents must be either in phase (0°) or antiphase (180 or -180°). The high coherence between signals also supports the idea of these dynamics being significant in the context of interactions between swell and coastal structures. This concept is crucial for understanding coastal dynamics in the region (Winter et al. 2017).

The presence of the observed wave pattern is influenced by reflection processes (Longuet-Higgins & Stewart 1962). These results are consistent with the fact that Bocagrande Beach exhibits a soft swell during the wet season, where energy is not completely dissipated, and reflection occurs. In addition, free IG waves acquire energy in the G shoaling zone and outer surf zone and can lose energy in the inner surf zone. As a result, reflected waves are usually IG, as they are not linked to short wave groups (de Bakker 2016).

Natural processes of wave group propagation and breaking generate IG waves. The work of Winter et al. (2017) demonstrated that the phase relation between η and current velocities (u and v) is essential for identifying the main wave types (leaky IG and edge waves) that interact with coastal settings, which can influence sediment transport. The same approach has been applied in previous studies (e.g. Huntley 1976, Holman 1981, Péquignet et al. 2009), as well as in this research.

In contrast to the relationship between IG waves and meteorology, instrumental analysis results indicate that tidal conditions do not influence IG wave transformation, regardless of whether it occurs during high tide or low tide. In other words, tidal conditions do not affect IG oscillations in the study area in terms of the type of IG wave present on each beach. Regarding the question of whether tide levels influence changes in the wave breaking line, this particular aspect could not be determined due to the spatial resolution of the instruments deployed on the studied beaches. An issue for future research to explore, which can be aided by high-resolution numerical modeling. In fact, the tides in the Colombian Caribbean are always less than 0.6 m. Nevertheless, the breaking point might change in beaches catalogued as microtidal but with tidal ranges greater (average 1.36 m) than those studied herein (Masselink & Short 1993). Regarding macrotidal beaches, their higher tide run values do affect IG waves due to the resulting modifications in breaking and energy transfer (Aagaard et al. 2013, Kularatne & Pattiaratchi 2014).

This research provides evidence that, in variable bathymetric conditions such as those present on beaches with intermediate features, like Bocagrande Beach, an entirely cross-shore array is insufficient for a comprehensive understanding of IG wave alongshore transformation and propagation. XWT data for the wet season indicate that edge waves did not form as they did during the dry season. However, during the wet season, important reflection processes were evident on Bocagrande Beach. To advance understanding of these processes, the deployment of an alongshore array is recommended. Additionally, researching the interaction between IG waves and sediment transport is suggested to improve knowledge of morphological evolution using techniques such as XWT and WTC.

CONCLUSIONS

In this research, two field campaigns were conducted during both climatic seasons on an intermediate-dissipative beach in the Colombian Caribbean. These field surveys aimed to assess the distribution of G and IG wave energy in the surf zone of the beach and to identify the patterns of IG waves. The results of this study lead to the following conclusions:

- The Iribarren number indicated that the surf zone at Bocagrande Beach is predominantly characterized by spilling breakers, with occasional plunging events.
- The dimensionless fall velocity parameter (Ω) classified the beach as an intermediate alongshore bar and rip system, with less pronounced bars during the dry season and a tendency to develop small rip currents.
- Spectral analysis showed G wave energy decreasing shoreward, while IG wave energy increased, prevailing in the alongshore velocity component (v).
- XWT and WTC analyses identified different IG wave patterns-including leaky, edge, and standing waves-with seasonal variations, demonstrating the efficiency of these methods in processing and interpreting hydrodynamic circulation in the surf zone.
- During the dry season, cross-shore and standing alongshore leaky waves were identified both nearshore and, in the zone, farthest from the shore, whereas in the zone closest to the shore, spectra revealed cross-shore and standing alongshore edge waves.
- During the wet season, leaky waves, both cross-shore and progressive alongshore, prevailed nearshore. Although wavelets are a traditional tool for IG wave characterization, the use of XWT and WTC represents a novel approach to identifying IG wave types.

Credit author contribution

J. Ruiz-Merchán: conceptualization, validation, methodology, formal analysis, writing-original draft, review and editing; J.C. Restrepo, L. Otero, J. Cueto & M. Conde-Frias: conceptualization, validation, methodology, formal analysis, writing-original draft, review; C. Tovio, M. Vega, A.M. Guerrero & M. Guerrero: data curation, formal analysis and review; B.K. Haus: formal analysis and review. All authors have read and accepted the published version of the manuscript.

Conflicts of interest

The authors declare that they have no conflicts of interest.

Data availability statement

The data presented in this study are available on request from the corresponding author.

ACKNOWLEDGMENTS

The authors thank the Ministerio de Ciencia Tecnología e Innovación and The Alfred C. Glassell, Jr. SUSTAIN (Surge-Structure-Atmosphere Interaction) Laboratory for the financial support. The authors also thank the Department of Research, Development, and Innovation at the Universidad del Norte and The Reef Institute.

REFERENCES

Aagaard, T. & Greenwood, B. 2008. Infragravity wave contribution to surf zone sediment transport - The role of advection. Marine Geology, 251: 1-14. doi: 10.1016/j.margeo.2008.01.017

Aagaard, T., Greenwood, B. & Hughes, M. 2013. Sediment transport on dissipative, intermediate and reflective beaches. Earth-Science Reviews, 124: 32-50. doi: 10.1016/j.earscirev.2013.05.002

Aucan, J. & Ardhuin, F. 2013. Infragravity waves in the deep ocean: An upward revision. Geophysical Research Letters, 40: 3435-3439. doi:10.1002/grl.50321

Austin, M. & Masselink, G. 2006. Observations of morphological change and sediment transport on a steep gravel beach. Marine Geology, 229: 59-77. doi: 10.1016/j.margeo.2006.02.003

Baldock, T.E. 2012. Dissipation of incident forced long waves in the surf zone-Implications for the concept of 'bound' wave release at short wave breaking. Coastal Engineering, 60: 276-285. doi: 10.1016/j.coastaleng.2011.11.002

Baldock, T. & Huntley, D. 2002. Long-wave forcing by the breaking of random gravity waves on a beach. Proceedings of the Royal Society of London - Series A: Mathematical, Physical and Engineering Sciences, 458: 2177-2201. doi: 10.1098/rspa.2002.0962

Baldock, T., Huntley, D., Bird, P., et al. 2000. Breakpoint generated surf beat induced by bichromatic wave groups. Coastal Engineering, 39: 213-242. doi: 10.1016/S0378-3839(99)00061-7

Battjes, J., Bakkenes, H., Janssen, T., et al. 2004. Shoaling of subharmonic gravity waves. Journal of Geophysical Research: Oceans, 109: 2003JC001863. doi: 10.1029/2003JC001863

Beach, R. & Sternberg, R. 1988. Suspended sediment transport in the surf zone: Response to cross-shore infragravity motion. Marine Geology, 80: 61-79. doi: 10.1016/0025-3227(88)90072-2

Booij, N., Ris, R. & Holthuijsen, L. 1999. A third-generation wave model for coastal regions: 1. Model description and validation. Journal of Geophysical Research: Oceans, 104: 7649-7666. doi: 10.1029/98JC02622

Bowen, A. & Inman, D. 1969. Rip currents: 2. Laboratory and field observations. Journal of Geophysical Research: Oceans and Atmospheres, 74: 5479-5490. doi: 10.1029/JC074i023p05479

Bowen, A. & Inman, D. 1971. Edge waves and crescentic bars. Journal of Geophysical Research: Oceans and Atmospheres, 76: 8662-8671. doi: 10.1029/JC076i036p08662

Bryan, K. & Bowen, A. 1996. Edge wave trapping and amplification on barred beaches. Journal of Geophysical Research: Oceans, 101: 6543-6552. doi: 10.1029/95JC03627

Carter, T.G., Liu, P.L-F. & Mei, C.C. 1973. Mass transport by waves and offshore sand bedforms. Journal of the Waterways, Harbors and Coastal Engineering Division Coasts, 99: 165-184. doi: 10.1061/awhcar.0000183

Coco, G., Burnet, T., Werner, B., et al. 2003. Test of self-organization in beach cusp formation. Journal of Geophysical Research: Oceans, 108: 2002JC001496. doi: 10.1029/2002JC001496

Coco, G., Burnet, T., Werner, B., et al. 2004. The role of tides in beach cusp development. Journal of Geophysical Research: Oceans, 109: 2003JC002154. doi: 10.1029/2003JC002154

Conde-Frias, M., Otero, L., Restrepo, J., et al. 2017a. Experimental analysis of infragravity waves in two eroded microtidal beaches. Acta Oceanologica Sinica, 36: 31-43. doi: 10.1007/s13131-017-1054-7

Conde-Frias, M., Otero, L., Restrepo, J., et al. 2017b. Swash oscillations in a microtidal dissipative beach. Journal of Coastal Research, 336: 1408-1422. doi: 10.2112/jcoastres-d-16-00147.1

Cueto, J. & Otero, L. 2020. Morphodynamic response to extreme wave events of microtidal dissipative and reflective beaches. Applied Ocean Research, 101: 102283. doi: 10.1016/j.apor.2020.102283

Cueto, J., Otero, L., Ospino-Ortiz, S., et al. 2022. The role of morphodynamics in predicting coastal flooding from storms on a dissipative beach with sea level rise conditions. Natural Hazards and Earth System Sciences, 22: 713-728. doi: 10.5194/nhess-22-713-2022

de Bakker, A.T.M. 2016. Infragravity-wave dynamics in shallow water: energy dissipation and role in sand suspension and transport. Dissertation, Utrecht University, Utrecht.

Goodfellow, B. & Stephenson, W. 2008. Role of infragravity energy in bar formation in a strong-wind bay: Observations from Seaford Beach, Port Phillip Bay, Australia. Geographical Research, 46: 208-223. doi: 10.1111/j.1745-5871.2008.00511.x

Grinsted, A., Moore, J. & Jevrejeva, S. 2004. Application of the cross wavelet transform and wavelet coherence to geophysical time series. Nonlinear Processes in Geophysics, 11: 561-566. doi: 10.5194/npg-11-561-2004

Guza, R. 1974. Excitation of edge waves and their role in the formation of beach cusps. Ph.D.dissertation, University of California, San Diego.

Guza, R. & Inman, D. 1975. Edge waves and beach cusps. Journal of Geophysical Research: Oceans, 80: 2997-3012. doi: 10.1029/JC080i021p02997

Guza, R. & Thornton, E. 1982. Swash oscillations on a natural beach. Journal of Geophysical Research: Oceans, 87: 483-491. doi: 10.1029/JC087iC01p00483

Guza, R. & Thornton, E. 1985. Observations of surf beat. Journal of Geophysical Research: Oceans, 90: 3161-3172. doi: 10.1029/JC090iC02p03161

Haring, R., Osborne, A. & Spencer, L. 1977. Extreme Wave parameters based on continental shelf storm wave records. Coastal Engineering, 1976: 151-170. doi: 10.1061/9780872620834.010

Henderson, S. & Bowen, A. 2003. Simulations of dissipative, shore-oblique infragravity waves. Journal of Physical Oceanography, 33: 1722-1732. doi: 10.1175/1520-0485(2003)033<1722:SODSIW>2.0.CO;2

Holman, R. 1981. Infragravity energy in the surf zone. Journal of Geophysical Research: Oceans, 86: 6442-6450. doi: 10.1029/JC086iC07p06442

Huntley, D. 1976. Long-period waves on a natural beach. Journal of Geophysical Research: Oceans and Atmospheres, 81: 6441-6449. doi: 10.1029/JC081i036p06441

Huntley, D. & Bowen, A. 1973. Field observations of edge waves. Nature, 243: 160-162. doi: 10.1038/243160a0

Huntley, D., Guza, R. & Thornton, E. 1981. Field observations of surf beat: 1. Progressive edge waves. Journal of Geophysical Research: Oceans, 86: 6451-6466. doi: 10.1029/JC086iC07p06451

Iribarren, C. & Nogales, C. 1949. Protection des ports. XVII, International Navigation Congress, Section II, Lisbon, pp. 31-80.

Kularatne, S. & Pattiaratchi, C. 2014. The role of infragravity waves in near-bed cross-shore sediment flux in the breaker zone. Journal of Marine Science and Engineering, 2: 568-592. doi: 10.3390/jmse2030568

Longuet-Higgins, M. & Stewart, R. 1962. Radiation stress and mass transport in gravity waves, with application to surf beats. Journal of Fluid Mechanics, 13: 481-504. doi: 10.1017/S0022112062000877

Longuet-Higgins, M. & Stewart, R. 1964. Radiation stresses in water waves; a physical discussion, with applications. Deep Sea Research and Oceanographic Abstracts, 11: 529-562. doi: 10.1016/0011-7471(64)90001-4

Masselink, G. 1995. Group bound long waves as a source of infragravity energy in the surf zone. Continental Shelf Research, 15: 1525-1547. doi: 10.1016/0278-4343(95)00037-2

Masselink, G. & Pattiaratchi, C. 2001. Seasonal changes in beach morphology along the sheltered coastline of Perth, Western Australia. Marine Geology, 172: 243-263. doi: 10.1016/S0025-3227(00)00128-6

Masselink, G. & Short, A. 1993. The effect of tide range on beach morphodynamics and morphology: a conceptual beach model. Journal of Coastal Research, 9: 785-800.

Melito, L., Parlagreco, L., Devoti, S., et al. 2022. Wave- and tide-induced infragravity dynamics at an intermediate-to-dissipative microtidal beach. Journal of Geophysical Research: Oceans, 127: e2021JC017980. doi: 10.1029/2021JC017980

Montaño-Muñoz, J. 2015. Influence of infragravity waves on the hydrodynamics of beaches. Ph.D. Thesis, Universidad Nacional de Colombia, Medellín.

Montaño-Muñoz, J., Osorio, A. & Otero, L. 2018. Swash excursion patterns at two contrasting beaches: Hollywood and Costa Verde beach, Colombia. Dyna, 85: 264-271. doi: 10.15446/dyna.v85n204.63363

Morawski, M., Różyński, G. & Szmytkiewicz, P. 2018. Calculation of wave run-up height in South Baltic Sea: case study at coastal research station at Lubiatowo, Poland. Archives of Hydro-Engineering and Environmental Mechanics, 65: 203-291. doi: 10.1515/heem-2018-0013

Munk, W. 1949. Surf beats. EOS. Transactions American Geophysical Union, 30: 849-854. doi: 10.1029/TR030i006p00849

Oltman-Shay, J. &. Guza, R. 1985. Infragravity edge wave observations on two California beaches. Ph.D. Thesis, University of California, San Diego.

Otero, L., Ortiz-Royero, J., Ruiz-Merchán, J., et al. 2016. Storms or cold fronts: what is really responsible for the extreme waves regime in the Colombian Caribbean coastal region? Natural Hazards and Earth System Sciences, 16: 391-401. doi: 10.5194/nhess-16-391-2016.

Péquignet, A., Becker, J., Merrifield, M., et al. 2009. Forcing of resonant modes on a fringing reef during tropical storm Man-Yi. Geophysical Research Letters, 36. doi: 10.1029/2008GL036259

Pomeroy, A., Lowe, R., Symonds, G., et al. 2012. The dynamics of infragravity wave transformation over a fringing reef. Journal of Geophysical Research: Oceans, 117: 2012JC008310. doi: 10.1029/2012JC008310

Posada, B. & Henao, W. 2008. Diagnóstico de la erosión en la zona costera del Caribe colombiano. Instituto de Investigaciones Marinas y Costeras "José Benito Vives de Andréis" [INVEMAR], Special Publication, No. 13.

Pruszak, Z., Różyński, G., Szmytkiewicz, M., et al. 2007. Field observation of edge waves and beach cusps on the South Baltic Sea coast. Journal of Coastal Research, 23: 846-860. doi: 10.2112/04-0293.1

Restrepo, J. & López, S. 2008. Morphodynamics of the Pacific and Caribbean deltas of Colombia, South America. Journal of South American Earth Sciences, 25: 1-21. doi: 10.1016/j.jsames.2007.09.002

Ruiz-Merchán, J., Otero, L., Conde, M., et al. 2019. Field observations of wave and current characteristics on a microtidal reflective beach. Journal of Coastal Research, 35: 1164-1184. doi: 10.2112/jcoastres-d-18-00120.1

Ruju, A., Lara, J. & Losada, I. 2012. Radiation stress and low-frequency energy balance within the surf zone: A numerical approach. Coastal Engineering, 68: 44-55. doi: 10.1016/j.coastaleng.2012.05.003

Received: June 16, 2025; Accepted: September 4, 2025

Schaffer, H. 1994. Edge waves forced by short-wave groups. Journal of Fluid Mechanics, 259. doi: 10.1017/S0022112094000066

Sharqawy, M., Lienhard, J. & Zubair, S. 2010. Thermophysical properties of seawater: A review of existing correlations and data. Desalination and water Treatment, 16: 354-380. doi: 10.5004/dwt.2010.1079

Stokes, G. 1850. On the effect of the internal friction of fluids on the motion of pendulums. Cambridge University Press, Cambridge. doi: 10.1017/CBO9780511702266.002

Symonds, G., Huntley, D. & Bowen, A. 1982. Two-dimensional surf beat: long wave generation by a time-varying breakpoint. Journal of Geophysical Research: Oceans, 87: 492-498. doi: 10.1029/JC087iC01p00492

Thomson, J., Elgar, S., Raubenheimer, B., et al. 2006. Tidal modulation of infragravity waves via nonlinear energy losses in the surfzone. Geophysical Research Letters, 33. doi: 10.1029/2005GL025514

Tucker, M. 1950. Surf beats: Sea waves of 1 to 5 min. period. Proceedings of the Royal Society of London - Series A: Mathematical and Physical Sciences, 202: 565-573. doi: 10.1098/rspa.1950.0120

Vidal, C., Losada, M., Medina, R., et al. 1995. Modelos de morfodinámica de playas. Ingeniería del Agua, 2: 55-74. doi: 10.4995/ia.1995.2665

Willmott, C., Ackleson, S., Davis, R., et al. 1985. Statistics for the evaluation and comparison of models. Journal of Geophysical Research: Oceans, 90: 8995-9005. doi: 10.1029/JC090iC05p08995

Winter, G., Lowe, R., Symonds, G., et al. 2017. Standing infragravity waves over an alongshore irregular rocky bathymetry. Journal of Geophysical Research: Oceans, 122: 4868-4885. doi: 10.1002/2016JC012242

Wright, L. & Short, A. 1984. Morphodynamic variability of surf zones and beaches: a synthesis. Marine Geology, 56: 93-118. doi: 10.1016/0025-3227(84)90008-2

Wright, L., Boon, J., Kim, S., et al. 1991. Modes of cross-shore sediment transport on the shoreface of the Middle Atlantic Bight. Marine Geology, 96: 19-51. doi: 10.1016/0025-3227(91)90200-N